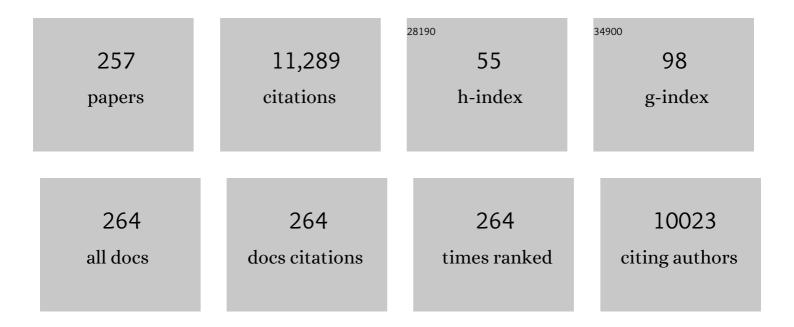
List of Publications by Year in descending order

Source: https://exaly.com/author-pdf/6182849/publications.pdf Version: 2024-02-01



ΗΙΔΕΗΙΡΟ Η ΙΙΔΑ

#	Article	IF	CITATIONS
1	Consensus Nomenclature for in vivo Imaging of Reversibly Binding Radioligands. Journal of Cerebral Blood Flow and Metabolism, 2007, 27, 1533-1539.	2.4	1,840
2	Dopaminergic neurons generated from monkey embryonic stem cells function in a Parkinson primate model. Journal of Clinical Investigation, 2005, 115, 102-109.	3.9	418
3	Measurement of absolute myocardial blood flow with H215O and dynamic positron-emission tomography. Strategy for quantification in relation to the partial-volume effect Circulation, 1988, 78, 104-115.	1.6	323
4	Error Analysis of a Quantitative Cerebral Blood Flow Measurement Using H ₂ ¹⁵ O Autoradiography and Positron Emission Tomography, with Respect to the Dispersion of the Input Function. Journal of Cerebral Blood Flow and Metabolism, 1986, 6, 536-545.	2.4	314
5	Noninvasive quantification of regional myocardial blood flow in coronary artery disease with oxygen-15-labeled carbon dioxide inhalation and positron emission tomography Circulation, 1991, 83, 875-885.	1.6	259
6	A Fully Automatic Multimodality Image Registration Algorithm. Journal of Computer Assisted Tomography, 1995, 19, 615-623.	0.5	254
7	(18)F-FDG accumulation in atherosclerotic plaques: immunohistochemical and PET imaging study. Journal of Nuclear Medicine, 2004, 45, 1245-50.	2.8	244
8	Myocardial efficiency during levosimendan infusion in congestive heart failure. Clinical Pharmacology and Therapeutics, 2000, 68, 522-531.	2.3	206
9	Early impairment of coronary flow reserve in young men with borderline hypertension. Journal of the American College of Cardiology, 1998, 32, 147-153.	1.2	195
10	A System for Cerebral Blood Flow Measurement Using an H215O Autoradiographic Method and Positron Emission Tomography. Journal of Cerebral Blood Flow and Metabolism, 1987, 7, 143-153.	2.4	167
11	Coronary Flow Reserve Is Impaired in Young Men With Familial Hypercholesterolemia. Journal of the American College of Cardiology, 1996, 28, 1705-1711.	1.2	167
12	A new strategy for the assessment of viable myocardium and regional myocardial blood flow using 15O-water and dynamic positron emission tomography Circulation, 1992, 86, 167-178.	1.6	159
13	The association between the Val158Met polymorphism of the catechol-O-methyl transferase gene and morphological abnormalities of the brain in chronic schizophrenia. Brain, 2006, 129, 399-410.	3.7	142
14	Role of blood flow in regulating insulin-stimulated glucose uptake in humans. Studies using bradykinin, [150]water, and [18F]fluoro-deoxy-glucose and positron emission tomography Journal of Clinical Investigation, 1996, 97, 1741-1747.	3.9	141
15	Evaluation of Regional Differences of Tracer Appearance Time in Cerebral Tissues Using [150]Water and Dynamic Positron Emission Tomography. Journal of Cerebral Blood Flow and Metabolism, 1988, 8, 285-288.	2.4	136
16	Arterial fraction of cerebral blood volume in humans measured by positron emission tomography. Annals of Nuclear Medicine, 2001, 15, 111-116.	1.2	129
17	Preoperative prediction of the outcome of coronary revascularization using positron emission tomography Circulation, 1992, 86, 1738-1742.	1.6	123
18	Regional Differences in Cerebral Vascular Response to Paco2 Changes in Humans Measured by Positron Emission Tomography. Journal of Cerebral Blood Flow and Metabolism, 2000, 20, 1264-1270.	2.4	121

#	Article	IF	CITATIONS
19	Glucose Uptake in the Chronically Dysfunctional but Viable Myocardium. Circulation, 1996, 93, 1658-1666.	1.6	121
20	Impaired Myocardium Regeneration With Skeletal Cell Sheets—A Preclinical Trial for Tissue-Engineered Regeneration Therapy. Transplantation, 2010, 90, 364-372.	0.5	118
21	Oxygen Extraction Fraction at Maximally Vasodilated Tissue in the Ischemic Brain Estimated from the Regional CO ₂ Responsiveness Measured by Positron Emission Tomography. Journal of Cerebral Blood Flow and Metabolism, 1988, 8, 227-235.	2.4	115
22	Long-term observation of auto-cell transplantation in non-human primate reveals safety and efficiency of bone marrow stromal cell-derived Schwann cells in peripheral nerve regeneration. Experimental Neurology, 2010, 223, 537-547.	2.0	107
23	Regional cerebral blood flow, blood volume, oxygen extraction fraction, and oxygen utilization rate in normal volunteers measured by the autoradiographic technique and the single breath inhalation method. Annals of Nuclear Medicine, 1995, 9, 15-21.	1.2	106
24	Myocardial Oxygen Consumption Is Unchanged but Efficiency Is Reduced in Patients With Essential Hypertension and Left Ventricular Hypertrophy. Circulation, 1999, 100, 2425-2430.	1.6	100
25	In Vivo Low Density Lipoprotein Oxidation Relates to Coronary Reactivity in Young Men. Journal of the American College of Cardiology, 1997, 30, 97-102.	1.2	98
26	Coronary Flow Reserve in Young Men With Familial Combined Hyperlipidemia. Circulation, 1999, 99, 1678-1684.	1.6	98
27	A Multicenter Validation of Regional Cerebral Blood Flow Quantitation Using [1231]Iodoamphetamine and Single Photon Emission Computed Tomography. Journal of Cerebral Blood Flow and Metabolism, 1996, 16, 781-793.	2.4	95
28	Hyperthyroidism Increases Brown Fat Metabolism in Humans. Journal of Clinical Endocrinology and Metabolism, 2014, 99, E28-E35.	1.8	95
29	Minimum cross-entropy reconstruction of PET images using prior anatomical information. Physics in Medicine and Biology, 1996, 41, 2497-2517.	1.6	92
30	Endogenous dopamine release induced by repetitive transcranial magnetic stimulation over the primary motor cortex: an [11C]raclopride positron emission tomography study in anesthetized macaque monkeys. Biological Psychiatry, 2004, 55, 484-489.	0.7	91
31	Widespread decrease of nicotinic acetylcholine receptors in Parkinson's disease. Annals of Neurology, 2006, 59, 174-177.	2.8	85
32	Design and evaluation of HEADTOME-IV, a whole-body positron emission tomograph. IEEE Transactions on Nuclear Science, 1989, 36, 1006-1010.	1.2	84
33	Monte Carlo and experimental evaluation of accuracy and noise properties of two scatter correction methods for SPECT. Physics in Medicine and Biology, 1996, 41, 2481-2496.	1.6	84
34	A Novel Mouse Model of Subcortical Infarcts with Dementia. Journal of Neuroscience, 2015, 35, 3915-3928.	1.7	82
35	A method to quantitate cerebral blood flow using a rotating gamma camera and iodine-123 iodoamphetamine with one blood sampling. European Journal of Nuclear Medicine and Molecular Imaging, 1994, 21, 1072-84.	2.2	81
36	Association between chronic stress-induced structural abnormalities in Ranvier nodes and reduced oligodendrocyte activity in major depression. Scientific Reports, 2016, 6, 23084.	1.6	80

#	Article	IF	CITATIONS
37	Design and Evaluation of a Positron Emission Tomograph. Journal of Computer Assisted Tomography, 1985, 9, 931-939.	0.5	76
38	Rapid Quantitative Measurement of CMRO2 and CBF by Dual Administration of 15O-Labeled Oxygen and Water During a Single PET Scan—a Validation Study and Error Analysis in Anesthetized Monkeys. Journal of Cerebral Blood Flow and Metabolism, 2005, 25, 1209-1224.	2.4	76
39	Photic Stimulation Study of Changing the Arterial Partial Pressure Level of Carbon Dioxide. Journal of Cerebral Blood Flow and Metabolism, 1995, 15, 111-114.	2.4	75
40	Quantitative assessment of regional myocardial blood flow with thallium-201 and SPECT*1. Journal of Nuclear Cardiology, 1998, 5, 313-331.	1.4	74
41	Coronary flow reserve is reduced in young men with IDDM. Diabetes, 1998, 47, 248-254.	0.3	74
42	A Determination of the Regional Brain/Blood Partition Coefficient of Water Using Dynamic Positron Emission Tomography. Journal of Cerebral Blood Flow and Metabolism, 1989, 9, 874-885.	2.4	71
43	Cerebral Blood Flow and Metabolism of Hyperperfusion after Cerebral Revascularization in Patients with Moyamoya Disease. Journal of Cerebral Blood Flow and Metabolism, 2012, 32, 2066-2075.	2.4	71
44	Quantitation of Regional Cerebral Blood Flow Corrected for Partial Volume Effect Using O-15 Water and PET: I. Theory, Error Analysis, and Stereologic Comparison. Journal of Cerebral Blood Flow and Metabolism, 2000, 20, 1237-1251.	2.4	70
45	Multicenter Evaluation of a Standardized Protocol for Rest and Acetazolamide Cerebral Blood Flow Assessment Using a Quantitative SPECT Reconstruction Program and Split-Dose ¹²³ 1-Iodoamphetamine. Journal of Nuclear Medicine, 2010, 51, 1624-1631.	2.8	69
46	Noninvasive Quantification of Regional Myocardial Metabolic Rate for Oxygen by Use of ¹⁵ O ₂ Inhalation and Positron Emission Tomography. Circulation, 1996, 94, 792-807.	1.6	69
47	Three-dimensional brain phantom containing bone and grey matter structures with a realistic head contour. Annals of Nuclear Medicine, 2013, 27, 25-36.	1.2	68
48	A Theoretical Model of Oxygen Delivery and Metabolism for Physiologic Interpretation of Quantitative Cerebral Blood Flow and Metabolic Rate of Oxygen. Journal of Cerebral Blood Flow and Metabolism, 2003, 23, 1314-1323.	2.4	67
49	Advances in multimodal neuroimaging: Hybrid MR–PET and MR–PET–EEG at 3T and 9.4T. Journal of Magnetic Resonance, 2013, 229, 101-115.	1.2	67
50	Gene Transfer of Hepatocyte Growth Factor Gene Improves Learning and Memory in the Chronic Stage of Cerebral Infarction. Hypertension, 2006, 47, 742-751.	1.3	65
51	Impaired free fatty acid uptake in skeletal muscle but not in myocardium in patients with impaired glucose tolerance: studies with PET and 14(R,S)-[18F]fluoro-6-thia-heptadecanoic acid. Diabetes, 1999, 48, 1245-1250.	0.3	63
52	Long-term effect of motor cortical repetitive transcranial magnetic stimulation induces. Annals of Neurology, 2004, 56, 77-85.	2.8	61
53	Influence of Cardiovascular Risk Status on Coronary Flow Reserve in Healthy Young Men. American Journal of Cardiology, 1997, 79, 1690-1692.	0.7	60
54	Quantitation of Regional Cerebral Blood Flow Corrected for Partial Volume Effect Using O-15 Water and PET: II. Normal Values and Gray Matter Blood Flow Response to Visual Activation. Journal of Cerebral Blood Flow and Metabolism, 2000, 20, 1252-1263.	2.4	59

#	Article	IF	CITATIONS
55	Combined PET/MRI: Multi-modality Multi-parametric Imaging Is Here. Molecular Imaging and Biology, 2015, 17, 595-608.	1.3	56
56	Comparison of myocardial blood flow during dobutamine-atropine infusion with that after dipyridamole administration in normal men. Journal of the American College of Cardiology, 2001, 37, 130-136.	1.2	54
57	High amyloidâ€Î² deposition related to depressive symptoms in older individuals with normal cognition: a pilot study. International Journal of Geriatric Psychiatry, 2016, 31, 920-928.	1.3	53
58	Gradual Carotid Artery Stenosis in Mice Closely Replicates Hypoperfusive Vascular Dementia in Humans. Journal of the American Heart Association, 2016, 5, .	1.6	50
59	Development of a GSO detector assembly for a continuous blood sampling system. IEEE Transactions on Nuclear Science, 2003, 50, 70-73.	1.2	48
60	Noninvasive Quantification of Regional Myocardial Metabolic Rate of Oxygen by ¹⁵ O ₂ Inhalation and Positron Emission Tomography. Circulation, 1996, 94, 808-816.	1.6	47
61	Quantification of nicotinic acetylcholine receptors in human brain using [1231]5-I-A-85380 SPET. European Journal of Nuclear Medicine and Molecular Imaging, 2003, 30, 1620-1629.	3.3	45
62	Quantitative mapping of basal and vasareactive cerebral blood flow using split-dose 1231-iodoamphetamine and single photon emission computed tomography. NeuroImage, 2006, 33, 1126-1135.	2.1	45
63	Absolute quantitation of myocardial blood flow with 201Tl and dynamic SPECT in canine: optimisation and validation of kinetic modelling. European Journal of Nuclear Medicine and Molecular Imaging, 2008, 35, 896-905.	3.3	45
64	Acceleration of Monte Carlo-based scatter compensation for cardiac SPECT. Physics in Medicine and Biology, 2008, 53, N277-N285.	1.6	45
65	Parametric imaging of myocardial blood flow with 150-water and PET using the basis function method. Journal of Nuclear Medicine, 2005, 46, 1219-24.	2.8	45
66	Rapid Quantitative <i>CBF</i> and <i>CMRO</i> ₂ Measurements from a Single <i>PET</i> Scan with Sequential Administration of Dual ¹⁵ O-Labeled Tracers. Journal of Cerebral Blood Flow and Metabolism, 2013, 33, 440-448.	2.4	41
67	Substantial Reduction of Parenchymal Cerebral Blood Flow in Mice with Bilateral Common Carotid Artery Stenosis. Scientific Reports, 2016, 6, 32179.	1.6	40
68	The use of magnetic resonance cell tracking to monitor endothelial progenitor cells in a rat hindlimb ischemic model. Biomaterials, 2012, 33, 2439-2448.	5.7	39
69	Development of Injectable O-15 Oxygen and Estimation of Rat OEF. Journal of Cerebral Blood Flow and Metabolism, 2003, 23, 671-676.	2.4	38
70	Evaluation of a commercial PET tomograph-based system for the quantitative assessment of rCBF, rOEF and rCMRO2 by using sequential administration of 15O-labeled compounds. Annals of Nuclear Medicine, 2002, 16, 317-327.	1.2	37
71	Interhemispheric functional disconnection because of abnormal corpus callosum integrity in bipolar disorder type II. BJPsych Open, 2016, 2, 335-340.	0.3	37
72	Intraperitoneal and intravenous deliveries are not comparable in terms of drug efficacy and cell distribution in neonatal mice with hypoxia–ischemia. Brain and Development, 2015, 37, 376-386.	0.6	35

#	Article	IF	CITATIONS
73	Reduction in camera-specific variability in [123I]FP-CIT SPECT outcome measures by image reconstruction optimized for multisite settings: impact on age-dependence of the specific binding ratio in the ENC-DAT database of healthy controls. European Journal of Nuclear Medicine and Molecular Imaging, 2016, 43, 1323-1336.	3.3	35
74	Dysregulation of RNF213 promotes cerebral hypoperfusion. Scientific Reports, 2018, 8, 3607.	1.6	34
75	Insulin increases blood volume in human skeletal muscle: studies using [150]CO and positron emission tomography. American Journal of Physiology - Endocrinology and Metabolism, 1995, 269, E1000-E1005.	1.8	33
76	Separation of input function for rapid measurement of quantitative CMRO2and CBF in a single PET scan with a dual tracer administration method. Physics in Medicine and Biology, 2007, 52, 1893-1908.	1.6	33
77	Resting-state synchrony between the retrosplenial cortex and anterior medial cortical structures relates to memory complaints in subjective cognitive impairment. Neurobiology of Aging, 2015, 36, 2145-2152.	1.5	33
78	Relationship between limb and muscle blood flow in man Journal of Physiology, 1996, 496, 543-549.	1.3	32
79	Use of a compact pixellated gamma camera for small animal pinhole SPECT imaging. Annals of Nuclear Medicine, 2006, 20, 409-416.	1.2	32
80	Delayed Postischemic Treatment With Fluvastatin Improved Cognitive Impairment After Stroke in Rats. Stroke, 2007, 38, 3251-3258.	1.0	32
81	Combined autologous cellular cardiomyoplasty using skeletal myoblasts and bone marrow cells for human ischemic cardiomyopathy with left ventricular assist system implantation: Report of a case. Surgery Today, 2009, 39, 133-136.	0.7	31
82	A New Approach of Weighted Integration Technique Based on Accumulated Images Using Dynamic PET and H ¹⁵ ₂ 0. Journal of Cerebral Blood Flow and Metabolism, 1991, 11, 492-501.	2.4	30
83	Insulin resistance in essential hypertension is characterized by impaired insulin stimulation of blood flow in skeletal muscle. Journal of Hypertension, 1998, 16, 211-219.	0.3	30
84	Non-invasive estimation of hepatic blood perfusion from H2 15O PET images using tissue-derived arterial and portal input functions. European Journal of Nuclear Medicine and Molecular Imaging, 2008, 35, 1899-1911.	3.3	29
85	Experimental Pig Model of Old Myocardial Infarction with Long Survival Leading to Chronic Left Ventricular Dysfunction and Remodeling as Evaluated by PET. Journal of Nuclear Medicine, 2011, 52, 761-768.	2.8	29
86	Effects of patient movement on measurements of myocardial blood flow and viability in resting 15O-water PET studies. Journal of Nuclear Cardiology, 2012, 19, 524-533.	1.4	29
87	Evaluation of penetration and scattering components in conventional pinhole SPECT: phantom studies using Monte Carlo simulation. Physics in Medicine and Biology, 2003, 48, 995-1008.	1.6	28
88	Implantation study of small-caliber "biotube―vascular grafts in a rat model. Journal of Artificial Organs, 2013, 16, 59-65.	0.4	28
89	The Leptomeningeal Ivy Sign on Fluid-Attenuated Inversion Recovery Images in Moyamoya Disease: Positron Emission Tomography Study. Cerebrovascular Diseases, 2013, 36, 19-25.	0.8	28
90	Effects of Magnetic Fields of up to 9.4 T on Resolution and Contrast of PET Images as Measured with an MR-BrainPET. PLoS ONE, 2014, 9, e95250.	1.1	28

#	Article	IF	CITATIONS
91	Anatomical Adjustments in Brain Positron Emission Tomography Using CT Images. Journal of Computer Assisted Tomography, 1988, 12, 363-367.	0.5	27
92	Reduced myocardial flow reserve relates to increased carotid intima-media thickness in healthy young men. Atherosclerosis, 2001, 156, 469-475.	0.4	27
93	A new reconstruction strategy for image improvement in pinhole SPECT. European Journal of Nuclear Medicine and Molecular Imaging, 2004, 31, 1166-72.	3.3	27
94	Validity of using a 3-dimensional PET scanner during inhalation of ¹⁵ O-labeled oxygen for quantitative assessment of regional metabolic rate of oxygen in man. Physics in Medicine and Biology, 2014, 59, 5593-5609.	1.6	26
95	A New PET Camera for Noninvasive Quantitation of Physiological Functional Parametric Images. , 1996, , 57-61.		26
96	Microstructural Differences in the Corpus Callosum in Patients With Bipolar Disorder and Major Depressive Disorder. Journal of Clinical Psychiatry, 2017, 78, 99-104.	1.1	26
97	Heart and brain circulation and CO ₂ in healthy men. Acta Physiologica, 2008, 193, 303-308.	1.8	25
98	Renal hemodynamics and fatty acid uptake: effects of obesity and weight loss. American Journal of Physiology - Endocrinology and Metabolism, 2019, 317, E871-E878.	1.8	25
99	Contribution of scatter and attenuation compensation to SPECT images of nonuniformly distributed brain activities. Journal of Nuclear Medicine, 2003, 44, 512-9.	2.8	25
100	Quantitative assessment of regional myocardial blood flow using oxygen-15-labelled water and positron emission tomography: a multicentre evaluation in Japan. European Journal of Nuclear Medicine and Molecular Imaging, 2000, 27, 192-201.	3.3	24
101	Activation of the Anterior Cingulate Gyrus by 'Green Odor': A Positron Emission Tomography Study in the Monkey. Chemical Senses, 2003, 28, 565-572.	1.1	24
102	Parametric renal blood flow imaging using [150]H2O and PET. European Journal of Nuclear Medicine and Molecular Imaging, 2009, 36, 683-691.	3.3	24
103	Design and characterization of a polymeric MRI contrast agent based on PVA for <i>in vivo</i> livingâ€cell tracking. Contrast Media and Molecular Imaging, 2010, 5, 309-317.	0.4	24
104	Magnetic Resonance-Based Attenuation Correction and Scatter Correction in Neurological Positron Emission Tomography/Magnetic Resonance Imaging—Current Status With Emerging Applications. Frontiers in Physics, 2020, 7, .	1.0	24
105	Intravenously delivered multilineage-differentiating stress enduring cells dampen excessive glutamate metabolism and microglial activation in experimental perinatal hypoxic ischemic encephalopathy. Journal of Cerebral Blood Flow and Metabolism, 2021, 41, 1707-1720.	2.4	24
106	Synthesis and autoradiographic localization of muscarinic cholinergic antagonist (+)N-[11C]methyl-3-piperidyl benzilate as a potent radioligand for positron emission tomography. Applied Radiation and Isotopes, 1999, 50, 521-525.	0.7	23
107	Non-invasive estimation of hepatic glucose uptake from [18F]FDG PET images using tissue-derived input functions. European Journal of Nuclear Medicine and Molecular Imaging, 2009, 36, 2014-2026.	3.3	23
108	A Physiologic Model for Recirculation Water Correction in CMRO ₂ Assessment with ¹⁵ O ₂ Inhalation PET. Journal of Cerebral Blood Flow and Metabolism, 2009, 29, 355-364.	2.4	23

#	Article	IF	CITATIONS
109	Use of T1-weighted/T2-weighted magnetic resonance ratio to elucidate changes due to amyloid β accumulation in cognitively normal subjects. NeuroImage: Clinical, 2017, 13, 209-214.	1.4	23
110	Analyzing powers and cross sections for (p, d) reactions on nuclei of N = 50–82. Nuclear Physics A, 1983, 393, 52-68.	0.6	22
111	Quantitative evaluation of neutral amino acid transport in cerebral gliomas using positron emission tomography and fluorine-18 fluorophenylalanine. European Journal of Nuclear Medicine and Molecular Imaging, 1996, 23, 889-895.	2.2	22
112	Preserved Acetazolamide Reactivity in Lacunar Patients with Severe White-Matter Lesions: ¹⁵ O-Labeled Gas and H ₂ O Positron Emission Tomography Studies. Journal of Cerebral Blood Flow and Metabolism, 2012, 32, 844-850.	2.4	22
113	Low amyloidâ€Î² deposition correlates with high education in cognitively normal older adults: a pilot study. International Journal of Geriatric Psychiatry, 2015, 30, 919-926.	1.3	22
114	A BGO Detector Unit for a Stationary High Resolution Positron Emission Tomograph. Journal of Computer Assisted Tomography, 1986, 10, 851-855.	0.5	21
115	Direct Experimental Evidence for Strong, Sequential, Two-Step, Transfer Processes in Allowed (p,t) Reactions. Physical Review Letters, 1981, 46, 810-812.	2.9	20
116	Effect of Intravenous Dipyridamole on Cerebral Blood Flow in Humans. Stroke, 1999, 30, 1616-1620.	1.0	20
117	Noise reduction in PET attenuation correction using non-linear Gaussian filters. IEEE Transactions on Nuclear Science, 2000, 47, 994-999.	1.2	20
118	Development of a phoswich detector for a continuous blood-sampling system. IEEE Transactions on Nuclear Science, 2001, 48, 1408-1411.	1.2	20
119	Long-Term <i>In Vivo</i> Magnetic Resonance Imaging Tracking of Endothelial Progenitor Cells Transplanted in Rat Ischemic Limbs and Their Angiogenic Potential. Tissue Engineering - Part A, 2011, 17, 2079-2089.	1.6	20
120	Reproducibility of Cerebral Blood Flow Assessment using a Quantitative SPECT Reconstruction Program and Split-Dose ¹²³ I-Iodoamphetamine in Institutions with Different <i>l³</i> -Cameras and Collimators. Journal of Cerebral Blood Flow and Metabolism, 2012, 32, 1757-1764.	2.4	20
121	Long-Term/Bioinert Labeling of Rat Mesenchymal Stem Cells with PVA-Gd Conjugates and MRI Monitoring of the Labeled Cell Survival after Intramuscular Transplantation. Bioconjugate Chemistry, 2014, 25, 1243-1251.	1.8	20
122	Estimation of Oxygen Metabolism in a Rat Model of Permanent Ischemia Using Positron Emission Tomography with Injectable 15O-O2. Journal of Cerebral Blood Flow and Metabolism, 2006, 26, 1577-1583.	2.4	19
123	Instrumentation and Methodology for Quantitative Pre-Clinical Imaging Studies. Current Pharmaceutical Design, 2001, 7, 1945-1966.	0.9	18
124	Effect of real-time weighted integration system for rapid calculation of functional images in clinical positron emission tomography. IEEE Transactions on Medical Imaging, 1995, 14, 116-121.	5.4	17
125	Quantitative evaluation of changes in binding potential with a simplified reference tissue model and multiple injections of [11C]raclopride. NeuroImage, 2009, 47, 1639-1648.	2.1	17
126	Use of [11C]acetate and [150]O2 PET for the assessment of myocardial oxygen utilization in patients with chronic myocardial infarction. European Journal of Nuclear Medicine and Molecular Imaging, 2001, 28, 334-339.	2.2	16

#	Article	IF	CITATIONS
127	Brain perfusion SPECT study with99mTc-bicisate: Clinical pitfalls and improved diagnostic accuracy with a combination of linearization and scatter-attenuation correction. Annals of Nuclear Medicine, 2001, 15, 123-129.	1.2	16
128	System design and development of a pinhole SPECT system for quantitative functional imaging of small animals. Annals of Nuclear Medicine, 2006, 20, 245-251.	1.2	16
129	Sequential PET estimation of cerebral oxygen metabolism with spontaneous respiration of ¹⁵ O-gas in mice with bilateral common carotid artery stenosis. Journal of Cerebral Blood Flow and Metabolism, 2017, 37, 3334-3343.	2.4	16
130	Early Detection of Cerebral Infarction After Focal Ischemia Using a New MRI Indicator. Molecular Neurobiology, 2019, 56, 658-670.	1.9	16
131	Verification of a semi-automated MRI-guided technique for non-invasive determination of the arterial input function in 15O-labeled gaseous PET. Nuclear Instruments and Methods in Physics Research, Section A: Accelerators, Spectrometers, Detectors and Associated Equipment, 2013, 702, 111-113.	0.7	15
132	Delayed atrophy in posterior cingulate cortex and apathy after stroke. International Journal of Geriatric Psychiatry, 2015, 30, 566-572.	1.3	15
133	Significant correlation between openness personality in normal subjects and brain myelin mapping with T1/T2-weighted MR imaging. Heliyon, 2017, 3, e00411.	1.4	15
134	Regional Myocardial Metabolic Rate of Oxygen Measured by O2-15 Inhalation and Positron Emission Tomography in Patients with Cardiomyopathy. Clinical Nuclear Medicine, 2001, 26, 41-49.	0.7	14
135	Optimal scan time of oxygen-15-labeled gas inhalation autoradiographic method for measurement of cerebral oxygen extraction fraction and cerebral oxygen metabolic rate. Annals of Nuclear Medicine, 2008, 22, 667-675.	1.2	14
136	Microstructural abnormalities in white matter and their effect on depressive symptoms after stroke. Psychiatry Research - Neuroimaging, 2014, 223, 9-14.	0.9	14
137	Development of in vivo tissue-engineered microvascular grafts with an ultra small diameter of 0.6Âmm (MicroBiotubes): acute phase evaluation by optical coherence tomography and magnetic resonance angiography. Journal of Artificial Organs, 2016, 19, 262-269.	0.4	14
138	Development of matrix metalloproteinase-targeted probes for lung inflammation detection with positron emission tomography. Scientific Reports, 2018, 8, 1347.	1.6	14
139	Marked changes in (p,t) analyzing powers for the isotopes of Zr, Mo, Ru, and Pd and strong, sequential, two-step transfer processes in both (p,t) and (t,p) reactions. Physical Review C, 1982, 25, 1050-1053.	1.1	13
140	Error analysis of table look-up method for cerebral blood flow measurement by123I-IMP brain SPECT: Comparison with conventional microsphere model method. Annals of Nuclear Medicine, 1995, 9, 75-80.	1.2	13
141	Effects of scatter correction on regional distribution of cerebral blood flow using I-123-IMP and SPECT. Annals of Nuclear Medicine, 1999, 13, 331-336.	1.2	13
142	F-18 fluorodeoxyglucose uptake and water-perfusable tissue fraction in assessment of myocardial viability. Annals of Nuclear Medicine, 2012, 26, 644-655.	1.2	13
143	Mutual effect of cerebral amyloid β and peripheral lymphocytes in cognitively normal older individuals. International Journal of Geriatric Psychiatry, 2017, 32, e93-e99.	1.3	13
144	Validation of the dual-table autoradiographic method to quantify two sequential rCBFs in a single SPET session with N -isopropyl-[123 I] p -iodoamphetamine. European Journal of Nuclear Medicine and Molecular Imaging, 2003, 30, 943-950.	3.3	12

#	Article	IF	CITATIONS
145	Left atrial versus left ventricular input function for quantification of the myocardial blood flow with nitrogen-13 ammonia and positron emission tomography. European Journal of Nuclear Medicine and Molecular Imaging, 2004, 31, 71-76.	3.3	12
146	Parametric imaging of myocardial viability using 15O-labelled water and PET/CT: comparison with late gadolinium-enhanced CMR. European Journal of Nuclear Medicine and Molecular Imaging, 2012, 39, 1240-1245.	3.3	12
147	Quantitative assessment of rest and acetazolamide CBF using quantitative SPECT reconstruction and sequential administration of 123I-iodoamphetamine: comparison among data acquired at three institutions. Annals of Nuclear Medicine, 2014, 28, 836-850.	1.2	12
148	Microstructural abnormality in white matter, regulatory <scp>T</scp> lymphocytes, and depressive symptoms after stroke. Psychogeriatrics, 2014, 14, 213-221.	0.6	12
149	Effect of scatter correction on the compartmental measurement of striatal and extrastriatal dopamine D 2 receptors using [123 I]epidepride SPET. European Journal of Nuclear Medicine and Molecular Imaging, 2004, 31, 644-654.	3.3	11
150	Use of a clinical MRI scanner for preclinical research on rats. Radiological Physics and Technology, 2009, 2, 13-21.	1.0	11
151	Development of motion correction technique for cardiac 15O-water PET study using an optical motion tracking system. Annals of Nuclear Medicine, 2010, 24, 1-11.	1.2	11
152	Breath-hold CT attenuation correction for quantitative cardiac SPECT. EJNMMI Research, 2012, 2, 33.	1.1	11
153	Cerebral blood flow and metabolism associated with cerebral microbleeds in small vessel disease. Annals of Nuclear Medicine, 2016, 30, 494-500.	1.2	11
154	Effect of Attenuation Correction on Regional Quantification Between PET/MR and PET/CT: A Multicenter Study Using a 3-Dimensional Brain Phantom. Journal of Nuclear Medicine, 2016, 57, 818-824.	2.8	11
155	System evaluation of automated production and inhalation of 15O-labeled gaseous radiopharmaceuticals for the rapid 15O-oxygen PET examinations. EJNMMI Physics, 2018, 5, 37.	1.3	11
156	Strong sequential transfer processes in 0+ → 0+ (p, t) reactions on Pb isotopes. Physics Letters, Section B: Nuclear, Elementary Particle and High-Energy Physics, 1981, 100, 232-235.	1.5	10
157	Understanding of cerebral energy metabolism by dynamic living brain slice imaging system with [18F]FDG. Neuroscience Research, 2005, 52, 357-361.	1.0	10
158	Three-dimensional SPECT reconstruction with transmission-dependent scatter correction. Annals of Nuclear Medicine, 2008, 22, 549-556.	1.2	10
159	Slowly progressive neuronal death associated with postischemic hyperperfusion in cortical laminar necrosis after high-flow bypass for a carotid intracavernous aneurysm. Journal of Neurosurgery, 2010, 112, 1254-1259.	0.9	10
160	Sensitivity of kinetic macro parameters to changes in dopamine synthesis, storage, and metabolism: A simulation study for [¹⁸ F]FDOPA PET by a model with detailed dopamine pathway. Synapse, 2011, 65, 751-762.	0.6	10
161	Quantification of regional cerebral blood flow in rats using an arteriovenous shunt and micro-PET. Nuclear Medicine and Biology, 2012, 39, 730-741.	0.3	10
162	The slow metabolism of L-[2-18F]-fluorophenylalanine in rat. Journal of Labelled Compounds and Radiopharmaceuticals, 1989, 27, 245-255.	0.5	9

#	Article	IF	CITATIONS
163	Accelerated median root prior reconstruction for pinhole single-photon emission tomography (SPET). Physics in Medicine and Biology, 2003, 48, 1957-1969.	1.6	9
164	Amyloid β deposition in subcortical stroke patients and effects of educational achievement: A pilot study. International Journal of Geriatric Psychiatry, 2019, 34, 1651-1657.	1.3	9
165	Elastic and inelastic scattering of polarized protons from the isotopes 104, 106, 108, 110Pd. Nuclear Physics A, 1983, 394, 413-427.	0.6	8
166	Construction of a simple focal-plane detector with high position resolution. Nuclear Instruments & Methods in Physics Research, 1984, 224, 432-439.	0.9	8
167	Parametric imaging in nuclear medicine. Annals of Nuclear Medicine, 1995, 9, 167-170.	1.2	8
168	Comparison of multi-ray and point-spread function based resolution recovery methods in pinhole SPECT reconstruction. Nuclear Medicine Communications, 2006, 27, 823-827.	0.5	8
169	3â€Tesla magnetic resonance angiographic assessment of a tissueâ€engineered smallâ€caliber vascular graft implanted in a rat. Journal of Biomedical Materials Research - Part B Applied Biomaterials, 2010, 92B, 156-160.	1.6	8
170	Measurement of Density and Affinity for Dopamine D2 Receptors by a Single Positron Emission Tomography Scan with Multiple Injections of [11C]raclopride. Journal of Cerebral Blood Flow and Metabolism, 2010, 30, 663-673.	2.4	8
171	Monte Carlo estimation of scatter effects on quantitative myocardial blood flow and perfusable tissue fraction using 3D-PET and ¹⁵ O-water. Physics in Medicine and Biology, 2012, 57, 7481-7492.	1.6	8
172	Quantification of myocardial blood flow using 201Tl SPECT and population-based input function. Annals of Nuclear Medicine, 2014, 28, 917-925.	1.2	8
173	Consensus Recommendations on the Use of 18F-FDG PET/CT in Lung Disease. Journal of Nuclear Medicine, 2020, 61, 1701-1707.	2.8	8
174	A Noninvasive Method for Quantifying Cerebral Metabolic Rate of Oxygen by Hybrid PET/MRI: Validation in a Porcine Model. Journal of Nuclear Medicine, 2021, 62, 1789-1796.	2.8	8
175	Evidence for dissociation of insulin stimulation of blood flow and glucose uptake in human skeletal muscle: studies using [150]H2O, [18F]fluoro-2-deoxy-D-glucose, and positron emission tomography. Diabetes, 1996, 45, 1471-1477.	0.3	8
176	Quantification of regional myocardial oxygen metabolism in normal pigs using positron emission tomography with injectable 150-02. European Journal of Nuclear Medicine and Molecular Imaging, 2010, 37, 377-385.	3.3	7
177	Quantitative assessment of regional cerebral blood flow by dynamic susceptibility contrast-enhanced MRI, without the need for arterial blood signals. Physics in Medicine and Biology, 2012, 57, 7873-7892.	1.6	7
178	Monte Carlo simulation of scintillation photons for the design of a high-resolution SPECT detector dedicated to human brain. Annals of Nuclear Medicine, 2012, 26, 214-221.	1.2	7
179	Imaging of the appearance time of cerebral blood using [150]H2O PET for the computation of correct CBF. EJNMMI Research, 2013, 3, 41.	1.1	7
180	Renal vascular resistance is increased in patients with kidney transplant. BMC Nephrology, 2019, 20, 437.	0.8	7

#	Article	IF	CITATIONS
181	Radiosynthesis of 15O-labeled hydrogen peroxide. Journal of Labelled Compounds and Radiopharmaceuticals, 1989, 27, 1167-1175.	0.5	6
182	Clinical Advantages of Interictal SPECT Coregistered to Magnetic Resonance Imaging in Patients with Epilepsy. Clinical Nuclear Medicine, 2001, 26, 334-339.	0.7	6
183	Regional Changes in Human Cerebral Blood Flow during Dipyridamole Stress: Neural Activation in the Thalamus and Prefrontal Cortex. NeuroImage, 2002, 16, 788-793.	2.1	6
184	Chapter 8 A coil for magnetic stimulation of the macaque monkey brain. Supplements To Clinical Neurophysiology, 2003, 56, 75-80.	2.1	6
185	Optimization of the width of the photopeak energy window in the TDCS technique for scatter correction in quantitative SPECT. IEEE Transactions on Nuclear Science, 2004, 51, 625-630.	1.2	6
186	Performance of list mode data acquisition with ECAT EXACT HR and ECAT EXACT HR+ positron emission scanners. Annals of Nuclear Medicine, 2006, 20, 189-194.	1.2	6
187	A method to measure PET scatter fractions for daily quality control. Medical Physics, 2009, 36, 4609-4615.	1.6	6
188	Influence from high and ultra-high magnetic field on positron range measured with a 9.4TMR-BrainPET. , 2010, , .		6
189	Influences of 3D PET scanner components on increased scatter evaluated by a Monte Carlo simulation. Physics in Medicine and Biology, 2017, 62, 4017-4030.	1.6	6
190	123I–Labeled oxLDL Is Widely Distributed Throughout the Whole Body in Mice. Nuclear Medicine and Molecular Imaging, 2018, 52, 144-153.	0.6	6
191	The renal blood flow reserve in healthy humans and patients with atherosclerotic renovascular disease measured by positron emission tomography using [150]H2O. EJNMMI Research, 2018, 8, 45.	1.1	6
192	Correction of Head Movement Using an Optical Motion Tracking System during PET in a Rhesus Monkey. , 2002, , 1-7.		6
193	Effects of insulin on blood flow and volume in skeletal muscle of patients with IDDM: studies using [150]H2O, [150]CO, and positron emission tomography. Diabetes, 1997, 46, 2017-2021.	0.3	6
194	Difference in anomalous0g+→0g+(p,t) analyzing powers for the isotones and partial cross sections for spin up and down. Physical Review C, 1982, 25, 1696-1698.	1.1	5
195	Drastic changes of (p,t) analyzing powers for the isotopesNi58,60,62,64and marked incident-energy dependence of the analyzing powers as evidence for strong, sequential, two-step processes. Physical Review C, 1984, 29, 328-331.	1.1	5
196	Energy dependence of (p,t) analyzing powers arising from strong, sequential, two-step processes withjdependence. Physical Review C, 1985, 31, 120-132.	1.1	5
197	A comparative study of three fast algorithms to estimate cerebral blood flow and distribution volume using N-isopropyl-p-(123I)iodoamphetamine and two SPECT scans. Physics in Medicine and Biology, 1995, 40, 1499-1515.	1.6	5
198	Development of a practical image-based scatter correction method for brain perfusion SPECT: comparison with the TEW method. European Journal of Nuclear Medicine and Molecular Imaging, 2005, 32, 1193-1198.	3.3	5

#	Article	IF	CITATIONS
199	Influence of residual oxygen-15-labeled carbon monoxide radioactivity on cerebral blood flow and oxygen extraction fraction in a dual-tracer autoradiographic method. Annals of Nuclear Medicine, 2009, 23, 363-371.	1.2	5
200	Three-dimensional quantitation of regional cerebral blood flow in mice using a high-resolution pinhole SPECT system and 1231-iodoamphetamine. Nuclear Medicine and Biology, 2011, 38, 1157-1164.	0.3	5
201	Advances in hybrid MR–PET at 3T and 9.4T in humans. Nuclear Instruments and Methods in Physics Research, Section A: Accelerators, Spectrometers, Detectors and Associated Equipment, 2013, 702, 16-21.	0.7	5
202	PET Quantification of Cerebral Oxygen Metabolism in Small Animals. Scientific World Journal, The, 2014, 2014, 1-7.	0.8	5
203	A structural model of age, grey matter volumes, education, and personality traits. Psychogeriatrics, 2016, 16, 46-53.	0.6	5
204	A non-invasive reference-based method for imaging the cerebral metabolic rate of oxygen by PET/MR: theory and error analysis. Physics in Medicine and Biology, 2021, 66, 065009.	1.6	5
205	Regional myocardial oxygen consumption estimated by carbon-11 acetate and positron emission tomography before and after repetitive ischemiaâ~†â~†â~†â~ Journal of Nuclear Cardiology, 2000, 7, 228-234.	1.4	4
206	Comparison of gd-dtpa-induced signal enhancements in rat brain c6 glioma among different pulse sequences in 3-tesla magnetic resonance imaging. Acta Radiologica, 2008, 49, 172-179.	0.5	4
207	Conceptual design of high resolution and quantitative SPECT system for imaging a selected small ROI of human brain. , 2009, , .		4
208	Optimization of transmission scan duration for 150 PET study with sequential dual tracer administration using N-index. Annals of Nuclear Medicine, 2010, 24, 413-420.	1.2	4
209	Asymmetrical intersection between the middle cerebral artery and rhinal vein suggests asymmetrical gustatory cortex location in rodent hemispheres. Neuroscience Letters, 2015, 589, 150-152.	1.0	4
210	Superfine Magnetic Resonance Imaging of the Cerebrovasculature Using Selfâ€Assembled Branched Polyethylene Glycol–Gd Contrast Agent. Macromolecular Bioscience, 2018, 18, e1700391.	2.1	4
211	Assessment of a digital and an analog PET/CT system for accurate myocardial perfusion imaging with a flow phantom. Journal of Nuclear Cardiology, 2022, 29, 1964-1972.	1.4	4
212	Magnetic Resonance Spectra of Hyperpolarized 129Xe in Human Blood and Living Rat Chest. Magnetic Resonance in Medical Sciences, 2003, 2, 189-194.	1.1	4
213	Silent ischemic lesion laterality in asymptomatic internal carotid artery stenosis relates to reduced cerebral vasoreactivity. , 2017, 8, 6.		4
214	Quantification in SPECT cardiac imaging. Journal of Nuclear Medicine, 2003, 44, 40-2.	2.8	4
215	Analyzing power as a probe for clarifying nuclear reaction mechanisms: Calculation of the two-step unbound channel contribution. Physical Review C, 1985, 31, 676-678.	1.1	3
216	Analysis of optimum diameter of orbit of transmission line source in positron emission tomograph. IEEE Transactions on Nuclear Science, 1989, 36, 1017-1019.	1.2	3

#	Article	IF	CITATIONS
217	New method for the synthesis of 15O-labeled carbon monoxide and 15O-labeled dioxide for rapid supply in clinical use. International Congress Series, 2004, 1265, 93-96.	0.2	3
218	Body-contour versus circular orbit acquisition in cardiac SPECT: Assessment of defect detectability with channelized Hotelling observer. Nuclear Medicine Communications, 2007, 28, 937-942.	0.5	3
219	Adequacy of a Compartment Model for CMRO ₂ Quantitation Using ¹⁵ O-Labeled Oxygen and PET: A Clearance Measurement of ¹⁵ O-Radioactivity Following Intracarotid Bolus Injection of ¹⁵ O-Labeled Oxyhemoglobin on <i>Macaca Fascicularis</i> , lournal of Cerebral Blood Flow and Metabolism, 2014, 34, 1434-1439.	2.4	3
220	Microstructural changes of the nucleus accumbens due to increase of estradiol level during menstrual cycle contribute to recurrent manic episodes—A single case study. Psychiatry Research - Neuroimaging, 2014, 221, 149-154.	0.9	3
221	Detection of brain amyloidâ€î² deposits due to the repetitive head trauma in a former karate player. Psychogeriatrics, 2019, 19, 276-281.	0.6	3
222	Evaluation of [18F]F-DPA PET for Detecting Microglial Activation in the Spinal Cord of a Rat Model of Neuropathic Pain. Molecular Imaging and Biology, 2022, 24, 641-650.	1.3	3
223	Count rate capability considerations and results for a positron emission tomograph. IEEE Transactions on Nuclear Science, 1989, 36, 1020-1024.	1.2	2
224	A convenient method for regional monoamine oxidase-a determination by [14C]clorgyline autoradiography. International Journal of Radiation Applications and Instrumentation Part B, Nuclear Medicine and Biology, 1992, 19, 619-626.	0.3	2
225	Accumulation of L-[2-(F-18)]fluorophenylalanine in peri-infarct area in a patient with acute cerebral infarction. Annals of Nuclear Medicine, 1994, 8, 213-217.	1.2	2
226	Development of injectable O-15 oxygen and its application for estimation of OEF. International Congress Series, 2004, 1265, 262-265.	0.2	2
227	A physiological model for cerebral oxygen delivery and consumption and effective oxygen diffusibility evaluated by PET. International Congress Series, 2004, 1265, 228-237.	0.2	2
228	Measurement of cerebral blood flow with dynamic susceptibility contrast MRI and comparison with O-15 positron emission tomography. International Congress Series, 2004, 1265, 150-158.	0.2	2
229	Determination of two-photon-excitation cross section for molecular isotope separation. Journal of Molecular Spectroscopy, 2012, 274, 14-21.	0.4	2
230	Binding of 11C-Pittsburgh compound-B correlated with white matter injury in hypertensive small vessel disease. Annals of Nuclear Medicine, 2017, 31, 227-234.	1.2	2
231	One-pot enzymatic synthesis of l-[3-11C]lactate for pharmacokinetic analysis of lactate metabolism in rat brain. Nuclear Medicine and Biology, 2018, 64-65, 28-33.	0.3	2
232	Vascular responses to abrupt blood flow change after bypass surgery for complex intracranial aneurysms. Acta Neurochirurgica, 2018, 160, 1945-1953.	0.9	2
233	Quantitative Assessment of Regional Myocardial Blood Flow with Clinical SPECT. Annals of Nuclear Cardiology, 2016, 2, 111-121.	0.0	2
234	Dependency of energy and spatial distributions of photons on edge of object in brain SPECT. Annals of Nuclear Medicine, 2003, 17, 99-106.	1.2	1

#	Article	IF	CITATIONS
235	Improved parametric images of blood flow and vascular volume by. International Congress Series, 2004, 1265, 79-83.	0.2	1
236	Accelerated 3D-OSEM image reconstruction using a Beowulf PC cluster for pinhole SPECT. Annals of Nuclear Medicine, 2007, 21, 537-543.	1.2	1
237	Evaluation of utility of asymmetric index for count-based oxygen extraction fraction on dual-tracer autoradiographic method for chronic unilateral brain infarction. Annals of Nuclear Medicine, 2009, 23, 533-539.	1.2	1
238	Shortening rCBF Measurement Interval in [150]H2O PET. , 2002, , 195-200.		1
239	Rapid CBF/CMRO2 measurement in a single PET scan with dual tracer administration. Journal of Cerebral Blood Flow and Metabolism, 2005, 25, S672-S672.	2.4	1
240	2.Essential and practical problems in attenuation correction : What can be done?. Japanese Journal of Radiological Technology, 2000, 56, 48-54.	0.0	1
241	In-plane resolution characteristics for a positron emission tomograph: Headtome IV. IEEE Transactions on Nuclear Science, 1989, 36, 1003-1005.	1.2	0
242	Determination of EC/IC bypass candidate by quantitative CBF measurement with by O-15 brain PET and I-123 IMP brain SPECT. International Congress Series, 2002, 1228, 63-70.	0.2	0
243	Therapeutic mechanism of repetitive transcranial magnetic stimulation (rTMS)—a monkey PET study. International Congress Series, 2004, 1264, 186-190.	0.2	0
244	Development of injectable O-15 oxygen and estimation of OEF in a transient ischemia–reperfusion rat model. International Congress Series, 2004, 1264, 197-201.	0.2	0
245	Future perspectives in in vivo quantitation of bio-physiological parameters. International Congress Series, 2004, 1264, 148-157.	0.2	0
246	Adenosine-induced myocardial flow reactivity in pig as assessed with O-15 water PET. International Congress Series, 2004, 1264, 117-125.	0.2	0
247	Improved parametric images of blood flow and vascular volume by cluster analysis in H215O brain PET study. International Congress Series, 2004, 1265, 79-83.	0.2	0
248	Development of high-resolution brain SPECT system using full-digital gamma camera with multiple position-sensitive PMTs. , 2015, , .		0
249	Development of a Hyperpolarized 129Xe System on 3T for the Rat Lungs. Magnetic Resonance in Medical Sciences, 2004, 3, 1-9.	1.1	0
250	Alteration of oxygen metabolism in MCA occlusion rat model by positron emission tomography with injectable O-15-oxygen. Journal of Cerebral Blood Flow and Metabolism, 2005, 25, S553-S553.	2.4	0
251	Development of sinogram-based estimation method of delay time of arterial input function with O-15 tracer and PET study. Journal of Cerebral Blood Flow and Metabolism, 2005, 25, S674-S674.	2.4	0
252	Cerebral Blood Volume Reactivity to Hypercapnia Measured by 11C-Labeled Carboxyhemoglobin and Positron Emission Tomography. , 1988, , 257-258.		0

#	Article	IF	CITATIONS
253	Assessment of Myocardial Viability Using 150-Water. Developments in Cardiovascular Medicine, 1996, , 241-262.	0.1	0
254	The Need for Quantitative SPECT in Clinical Brain Examinations. , 2016, , 17-38.		0
255	Mismatch cases between clinical finding and image finding on ¹⁵ O gas PET/CT study caused by misregistration of PET data relative to CT-based attenuation maps. No Junkan Taisha = Cerebral Blood Flow and Metabolism, 2016, 27, 215-224.	0.1	Ο
256	2089-P: Regional Renal Hemodynamics and Fatty Acid Uptake: Effects of Obesity and Weight Loss. Diabetes, 2019, 68, 2089-P.	0.3	0
257	Quantitative Assessment of Regional Myocardial Blood Flow with Clinical SPECT. Annals of Nuclear Cardiology, 2016, 2, 111-121.	0.0	0